Anal. Chem. **2002,** *74,* 5121−5131

Fluorescence Correlation Spectroscopy Excited with a Stationary Interference Pattern for Capillary Electrophoresis

Tsuyoshi Sonehara,* Kyoko Kojima, and Takashi Irie

Hitachi, Ltd., Central Research Laboratory, 1-280, Higashi-koigakubo Kokubunji-shi, Tokyo 185-8601, Japan

Using a combination of capillary electrophoresis (CE) and patterned fluorescence correlation spectroscopy (patterned FCS), we have developed a new technique for performing electrophoretic analysis independently of the initial length of injected analyte plugs. In this technique, which is abbreviated as CE/patterned FCS, fluorescent analyte molecules dispersed continuously in a capillary migrate through a stationary interference pattern created by two intersecting excitation laser beams, and their fluorescence emission is monitored. We prove theoretically that the power spectrum of fluctuations in the fluorescence intensity gives a virtual electropherogram. The profile of the electropherogram and the number of theoretical plates are in general obtained by using analytical methods. Characterizing the capillary length within the excitation beams as the effective length, we compare CE/patterned FCS with conventional CE. Numerical simulations on capillary gel electrophoresis of DNA predict that the optimized CE/patterned FCS is superior to conventional CE when the effective length is shorter than 1 cm. The experimental feasibility of this technique is demonstrated in the fluorometry of TOTO-1-stained DNA. For an effective length of 740 μm, a maximum number of plates of 7400, and a resolution of 1.0 were obtained with a one-component injection of pUC18 DNA and a two-component injection of pUC 18 DNA and λ DNA, respectively.

Capillary electrophoresis (CE) with laser-induced fluorescence detection (LIF) is widely used as a fundamental technique for analyzing biological molecules because of its high sensitivity, speed, and possibility of automation. To enhance the speed of analysis, various CE/LIF systems have been developed using short separation columns with an effective length of few centimeters.[1−11] For such a short effective length, the initial length of injected analyte plugs (injection length) becomes an important factor limiting the column efficiency. To obtain the shortest analyte plugs, Jorgensen and co-workers developed optical-gating injection.[1,2] Although this technique can generate very short analyte plugs, available excitation source and labeling fluorophore are limited because efficient photobleaching is required. Manz and co-workers introduced sample injection systems integrated on microfabricated planar chips for CE.[3−6] Such systems referred to as double-T or cross injectors have become a standard platform for rapid CE. These injectors can generate analyte plugs as short as those obtained by optically gating. Nevertheless, the injection length in many cases is the predominant concern for zone broadening in CE using columns shorter than 1 cm.[6,11] Recently, Manz and co-workers developed a new detection technique for CE/LIF, called Shah convolution Fourier transform detection (SCOFT).[12,13] In this technique, the spectra of electrophoretic mobilities are given as a temporal Fourier transform of the fluorescence intensity from a periodic excitation pattern. Although SCOFT is a unique method, it is not free from the problem of the injection length, since the pitch of the excitation pattern should be larger than the injection length for efficient signal generation.

There are a few techniques for performing electrophoretic analysis independently of the injection length. Chu and Wang combined gel electrophoresis with the movement of fluorescence pattern after photobleaching (MOFPAP).[14−17] Although the MOFPAP technique can measure the electophoretic mobility of analyte molecules dispersed continuously in the gel, this technique has the same limitations as the optical-gating technique because photobleaching is required. Several groups have combined CE

* To whom correspondence should be addressed. E-mail: sonehara@crl.hitachi.co.jp. Fax: +81−42−327−7751.

(1) Monnig, C. A.; Jorgenson, J. W. *Anal. Chem*. **1991**, *63*, 802−807.
(2) Moore, A. W., Jr.; Jorgenson, J. W. *Anal. Chem*. **1993**, *65*, 3550−3560.
(3) Manz, A.; Harrison, D. J.; Verpoorte, E. M. J.; Fettinger, J. C.; Paulus, A.; Lüdi, H.; Widmer, H. M. *J. Chromatogr.* **1992**, *593*, 253−258.
(4) Harrison, D. J.; Manz, A.; Fan, Z.; Lüdi, H.; Widmer, H. M. *Anal. Chem*. **1992**, *64*, 1926−1932.
(5) Harrison, D. J.; Fluri, K.; Seiler, K.; Fan, Z.; Effenhauser, C. S.; Manz, A. *Science* **1993**, *261*, 895−897.
(6) Effernhauser, C. S.; Manz, A.; Widmer, H. M. *Anal. Chem*. **1993**, *65*, 2637−2642.
(7) Jacobson, S. C.; Hergenröder, R.; Koutny, L. B.; Ramsey, J. M. *Anal. Chem*. **1994**, *66*, 1114−1118.
(8) Woolley, A. T.; Mathies, R. A. *Anal. Chem*. **1995**, *67*, 3676−3680.
(9) Bousse, L.; Dubrow, B.; Ulfelder, K. In *Micro Total Analysis Sistems '98*; Harrison, D. J., van den Berg, A., Eds.; Kluwer Academic Publishers: Dordrecht, The Netherlands, 1998; pp 271−275.
(10) Müller, O.; Minarik, M.; Foret, F. *Electrophoresis* **1998**, *19*, 1436−1444.
(11) Jacobson, S. C.; Culbertson, C. T.; Daler, J. E.; Ramsey, J. M. *Anal. Chem*. **1998**, *70*, 3476−3480.
(12) Crabtree, H. J.; Kopp, M. U.; Manz, A. *Anal. Chem*. **1999**, *71*, 2130−2138.
(13) Kwok, Y. C.; Manz, A. *Electrophoresis* **2001**, *22*, 222−229.
(14) Wang, Z.; Chu, B. *Phys. Rev. Lett*. **1989**, *63*, 2528−2531.
(15) Chu, B.; Wang, Z.; Wu, C. *Biopolymers* **1989**, *28*, 1491−1494.
(16) Wu, C.; Wang, Z.; Chu, B. *Biopolymers* **1990**, *29*, 491−500.
(17) Chu, B.; Wang, Z. *Electrophoresis* **1992**, *13*, 536−541.

10.1021/ac0201326 CCC: $22.00
Published on Web 08/23/2002

with the single-molecule detection (SMD) technique.[18−20] CE coupled with SMD, where individual analyte molecules are observed separately, is also independent of the injection length.

An alternative technique for CE that is not affected by the injection length is fluorescence correlation spectroscopy (FCS). FCS is a nonperturbative technique, which utilizes fluctuations in the fluorescence intensity, and unlike MOFPAP it does not require photobleaching.[21−27] Because the correlation function of the fluctuations varies with the flow velocity, FCS is applicable to electrophoresis.[24] Additionally, FCS offers a wider dynamic range on the analyte concentration than SMD does. Orden and Keller succeeded in performing multicomponent analysis by using a combination of CE and FCS (CE/FCS).[28] However, in conventional CE/FCS with a single detection volume, the peak of the correlation function is always positioned at lagtime 0 and only its shape changes, owing mainly to the change of the electrophoretic velocity. Hence, excellent discrimination between analytes with the same sign charges and close electrophoretic mobilties is difficult.

Recently, Brinkmeier et al. improved the FCS flow velocimetry by producing cross-correlation of fluctuations in the fluorescence intensities from two closely separated detection volumes.[29] In this technique, which is referred to as two-beam fluorescence cross-correlation spectroscopy (two-beam FCCS), the peak of the correlation function shifts in inverse proportion to the flow velocity. By using two-beam FCCS for CE separations, LeCaptain and Orden succeeded in resolving two components.[30] On the other hand, as early as 1978, Asai and Ando suggested a way to improve the FCS flow velocimetry by creating a stationary interference pattern of two intersecting excitation beams.[31,32] We refer to this modified FCS as patterned FCS, according to Hansen et al., who developed this technique to determine the diffusion coefficient of analytes.[33] In patterned FCS with an analyte flow, the correlation function is modulated at a frequency commensurate with the flow velocity. Thus, patterned FCS improves CE/FCS as well as two-beam FCCS. Furthermore, patterned FCS requires only one fluorescence detector, whereas two are required in two-beam FCCS. Despite this potential, the coupling of patterned FCS and CE has not been studied in detail.

In this paper, we describe a new combination of CE and patterned FCS, which is abbreviated as CE/patterned FCS, for performing electrophoretic analysis. The general principles and theoretical analysis are presented. While at first glance this technique is similar to SCOFT, it is no longer affected by the injection length. Moreover, the power spectrum of fluctuations in the fluorescence intensity gives a virtual electropherogram, which cannot be obtained in conventional CE/FCS. The number of theoretical plates obtained by CE/patterned FCS is compared with that obtained by conventional CE based on numerical simulations. Additionally, the sensitivity of this technique is discussed. Finally, experimental results are demonstrated on the fluorometry of TOTO-1-stained pUC18 DNA and λ DNA.

The first theoretical calculation of correlation functions in patterned FCS with an analyte flow was carried out by Asai and Ando.[31,32] However, they have yet to publish their results on the deviation. Thus, we introduce calculations that we carried out independently. Ando and Asai's calculations are based on ref 22, whereas ours are based on ref 24. The results are essentially equivalent.

THEORY

Basic Definitions and Relations. Fluctuations in the fluorescence intensity are seen experimentally as fluctuations in the photocurrent generated in a fluorescence detector. We postulate a dilute solution containing a single fluorescent analyte illuminated by a stationary excitation pattern, fluorescence emission from which is monitored using a photomultiplier tube (PMT) or a photodiode (PD) as the detector. If the photobleaching of the fluorophore is neglected, the photocurrent of the detector can be written as

$$i(t) = geQ\Phi\sigma \int \phi(\mathbf{r})C(\mathbf{r},t)\, \mathrm{d}\mathbf{r} \qquad (1)$$

where σ is the absorption cross section of the analyte molecule, Φ is the fluorescence quantum yield of the analyte, Q is the quantum efficiency of the detector, e is the elementally charge, g is the current gain of the detector, $\phi(\mathbf{r})$ is the molecule detection efficiency (MDE), which is defined as the product of the photon flux density profile of the excitation beam and the fluorescence collection efficiency profile of the detection optics, and $C(\mathbf{r},t)$ is the analyte concentration at position $\mathbf{r}$ and time t. The photocurrent fluctuations arising from concentration fluctuations are given by

$$\delta i(t) \equiv i(t) - \langle i \rangle = geQ\Phi\sigma \int \phi(\mathbf{r})\delta C(\mathbf{r},t)\, \mathrm{d}\mathbf{r} \qquad (2)$$

where $\langle\ \rangle$ denotes the ensemble average, and $\delta C(\mathbf{r},t) = C(\mathbf{r},t) - \langle C(\mathbf{r},t)\rangle$. The detection volume is defined by

$$v \equiv \{\int \phi(\mathbf{r})\, \mathrm{d}\mathbf{r}\}^2 / \int \{\phi(\mathbf{r})\}^2\, \mathrm{d}\mathbf{r} \qquad (3)$$

then we obtain

$$\langle i\rangle^2 / \langle \delta i^2 \rangle = \langle n \rangle = \bar{C}v \qquad (4)$$

(18) Castro, A.; Shera, E. B. *Anal. Chem.* **1995**, *67*, 3181−3186.
(19) Chen, D. Y.; Dovichi, N. J. *Anal. Chem.* **1996**, *68*, 690−696.
(20) Shortreed, M. R.; Li, H.; Huang, W.-H.; Yeung, E. S. *Anal. Chem.* **2000**, *72*, 2879−2885.
(21) Magde, D.; Elson, E.; Webb, W. W. *Phys. Rev. Lett.* **1972**, *29*, 705−708.
(22) Elson, E. L.; Magde, D. *Biopolymers* **1974**, *13*, 1−27.
(23) Aragón, S. R.; Pecora, R. *Biopolymers* **1975**, *14*, 119−138.
(24) Berne, B. J.; Pecora, R. *Dynamic Light Scattering: With Applications to Chemistry, Biology, and Physics*; Dover: New York, 2000; Section 6. 6.
(25) Magde, D.; Webb, W. W.; Elson, E. L. *Biopolymers* **1978**, *17*, 361−376.
(26) Hattori, M.; Shimizu, H.; Yokoyama, H. *Rev. Sci. Instrum.* **1996**, *67*, 4064−4071.
(27) Maiti, S.; Haupts, U.; Webb, W. W. *Proc. Natl. Acad. Sci. U.S.A.* **1997**, *94*, 11753−11757.
(28) Orden, A. V.; Keller, R. A. *Anal. Chem.* **1998**, *70*, 4463−4471.
(29) Brinkmeier, M.; Dörre, K.; Stephan, J.; Eigen, M. *Anal. Chem.* **1999**, *71*, 609−616.
(30) LeCaptain, D. J.; Orden, A. V. *Anal. Chem.* **2002**, *74*, 1171−1176.
(31) Asai, H.; Ando, T. Japanese Unexamined Patent Publication, Sho-53-40586, 1978.
(32) Asai, H.; Ando, T. Unpublished work in the Department of Physics, Waseda University, Tokyo, Japan, 1976. (The private communication from Ando was received Octover 20, 2001). Present address: Hiroshi Asai, Department of Physics, Waseda University, 3-4-1, Okubo, Shinjuku-ku, Tokyo 169-0072, Japan, E-mail: asai@mn.waseda.ac.jp; Toshio Ando, Faculty of Science, Kanazawa University, Kakuma-machi Kanazawa 920-1192, Japan, E-mail: tando@kenroku.kanazawa-u.ac.jp
(33) Hansen, R. L.; Zhu, X. R.; Harris, J. M. *Anal. Chem.* **1998**, *70*, 1281−1287.

where n is the number of analyte molecules in the detection volume and $\bar{C} \equiv \langle C(\mathbf{r},t)\rangle$.[27] According to ref 24, we introduce the normalized correlation function of $\delta i(t)$ by

$$G(t) \equiv \langle \delta i(0)\delta i(t)\rangle / \langle \delta i^2\rangle \tag{5}$$

While this correlation function is the leading element in conventional FCS, including patterned FCS, in our CE/patterned FCS, the power spectrum,[34] another fundamental quantity in fluctuation analysis, plays the central role. The power spectrum of $\delta i(t)$ at frequency f is defined by[35]

$$S(f) \equiv \lim_{T\to\infty}\left\langle \frac{2|\delta i_T(f)|^2}{T}\right\rangle \tag{6}$$

where $\delta i_T(f) \equiv \int_{-T/2}^{T/2} \delta i(t)\, \exp(-2\pi ftj)\, \mathrm{d}t$. The term between brackets in eq 6, $2|\delta i_T(f)|^2/T$, is called a periodogram. An averaged periodogram gives the power spectrum. From the Wiener–Khintchine theorem, $G(t)$ and $S(f)$ are related as follows:[36]

$$S(f) = 4\langle \delta i^2\rangle \int_0^\infty \mathrm{G}(t)\, \cos(2\pi ft)\, \mathrm{d}t \tag{7}$$

Fluorescence Correlation for Patterned Excitation. Consider two coherent excitation laser beams that propagate on the xy-plane in symmetry to the y-axis and intersect with each other at the origin at angle θ. These two beams have an identical elliptic Gaussian intensity profile of $1/e^2$ diameter L orthogonal to the z-axis and H parallel to the z-axis. Interference between the two intersecting beams yields an excitation profile with a Gaussian envelope that changes periodically along the x-axis. The pitch of the interference pattern is given by[33]

$$p = \lambda/2\, \sin(\theta/2) \tag{8}$$

here, λ is the laser wavelength in the solution. The fluorescence emission from the detection volume is monitored along the z-axis through a slit with a Gaussian transmittance profile in the y-direction of $1/e^2$ width W. If $\cos(\theta/2) \cong 1$ and $W \sin(\theta/2) \ll L$, we can express the MDE by

$$\phi(\mathbf{r}) = \phi_0 \exp\left(-\frac{8x^2}{L^2}\right)\left\{\cos\left(\frac{2\pi x}{p}\right) + 1\right\} \exp\left(-\frac{8y^2}{W^2}\right) \exp\left(-\frac{8z^2}{H^2}\right) \tag{9}$$

We specialize to the case of analyte molecules uniformly flowing along the x-axis at velocity V and assume that

$$p \ll L \tag{10}$$

$$4D/V \ll L, \quad W^2/L, \quad H^2/L \tag{11}$$

where D is the diffusion coefficient of the analyte. Then, $G(t)$ for $\phi(\mathbf{r})$ in eq 9 is approximated by

$$G(t) = \frac{1}{3}\exp\left\{-\frac{4V^2}{L^2}t^2 - D\left(\frac{2\pi}{p}\right)^2 t\right\}\cos\left(\frac{2\pi V}{p}t\right) + \frac{2}{3}\exp\left(-\frac{4V^2}{L^2}t^2\right) \tag{12}$$

The derivation of eq 12 is described in the Appendix. As shown in eq 12, an oscillating term, which has never been observed in conventional FCS with a stationary excitation pattern, appears in patterned FCS with an analyte flow. Note that the right-hand side of eq 12 is independent of W and H. Taking this fact into account, even though the slit has a square transmittance profile of width W, which is experimentally more available, the result expressed by eq 12 would not change as long as eq 11 is satisfied.

Here we give the mean photocurrent, $\langle i\rangle$, and the detection volume, v, for the MDE given by eq 9. Substituting eq 9 into eqs 1 and 3 gives

$$\langle i\rangle = \frac{\pi^{3/2}}{16\sqrt{2}} geQ\Phi\sigma\phi_0\bar{C}LWH \tag{13}$$

$$v = \frac{\pi^{3/2}}{8}LWH \tag{14}$$

Virtual Electropherogram. The power spectrum of photocurrent fluctuations in patterned FCS with an analyte flow is obtained by substituting eq 12 into eq 7. The result is expressed by

$$S(f) = \frac{\sqrt{\pi}L}{6V}\langle \delta i^2\rangle\left\{K\left(\frac{\pi L}{2V}\left(f - \frac{V}{p}\right), \left(\frac{p_0}{p}\right)^2\right) + K\left(\frac{\pi L}{2V}\left(f + \frac{V}{p}\right), \left(\frac{p_0}{p}\right)^2\right) + 4\exp\left(-\frac{\pi^2L^2}{4V^2}f^2\right)\right\} \tag{15}$$

where $K(x, y)$ is a Voigt function defined by

$$K(x,y) \equiv \frac{y}{\pi}\int_{-\infty}^{+\infty}\frac{\exp(-z^2)}{y^2 + (x-z)^2}\,\mathrm{d}z \tag{16}$$

and p_0 is a characteristic pitch defined by

$$p_0 \equiv \pi\sqrt{DL/V} \tag{17}$$

Since $K(x, y)$ is a function with a peak at $x = 0$, the first term in the braces of eq 15 gives a peak at the oscillation frequency of

(34) More precisely, "one-sided power spectral density function". In this paper, we use "power spectrum" to eliminate redundancy.

(35) Stark, H.; Woods, J. W. *Probability, Random Processes, and Estimation Theory for Engineers*, 2nd ed.; Prentice-Hall: Upper Saddle River, NJ, 1994; Chapter 10.

(36) Bendat, J. S.; Piersol, A. G. *Measurement and Analysis of Random Data*; John Wiley & Sons: New York, 1966; Chapter 3.

G(t), which is defined by

$$f_0 \equiv V/p \tag{18}$$

The full width at half-maximum (fwhm) of this peak is approximated by[37]

$$w_{1/2} = (4V/\pi L)\eta((p_0/p)^2) \tag{19}$$

where

$$\eta(y) \equiv y + \frac{0.8325 + 0.33049y}{1 + 0.92857y + 0.45814y^2} \tag{20}$$

If $w_{1/2} \ll V/p$, a peak at $f = f_0$ is clearly observed in the $S(f)$ curve and it does not overlap with the peaks at $f = -f_0$ and 0 arising from the second and third terms in the braces of eq 15. In this case, except for the vicinity of $f = 0$, eq 15 is simplified to

$$S(f) = \frac{\sqrt{\pi}L}{6V}\langle \delta i^2 \rangle K\left(\frac{\pi L}{2V}(f - f_0), \left(\frac{p_0}{p}\right)^2\right) \tag{21}$$

In the case of electrophoretically driven flow, f_0 is written by

$$f_0 = \mu E/p \tag{22}$$

where μ is the apparent mobility of the analyte, which is the sum of the electrophoretic mobility and the electroosmotic mobility, and E is the electric field. From eq 22, the peak position of $S(f)$ is commensurate with the analyte mobility. Hence, the power spectrum of the photocurrent fluctuations gives a virtual electropherogram. The transverse of conventional electropherograms obtained by single-point detection is time, whereas that of the virtual electropherogram is frequency proportional to mobility. Hence, electropherograms in CE/patterned FCS correspond more closely to fluorescence images in slab gel electrophoresis.

When the sample contains multicomponent fluorescent analytes, the power spectrum of the photocurrent fluctuations would be a superposition of the spectra observed for samples containing each component exclusively. Under adequate conditions, we should observe the same number of separate peaks as the number of components at positions commensurate with the mobilities of the analytes.

Separation Efficiency. The efficiency of CE systems is generally evaluated in terms of the number of theoretical plates. Characterizing the $S(f)$ curve as an electropherogram, we can define the number of theoretical plates in CE/patterned FCS by[38]

$$N \equiv 8 \ln 2(f_0/w_{1/2})^2 \tag{23}$$

Substitution of eq 19 into eq 23 gives

$$N = \frac{\ln 2}{2}\frac{(p_0/p)^2}{\{\eta((p_0/p)^2)\}^2}\frac{VL}{D} \tag{24}$$

Figure 1 shows the relationship between the normalized values of N and p. The normalization factor for N is defined by

$$N_{\max} \equiv VL/6.38D \tag{25}$$

The curve shows that if all the parameters except for p are fixed, the number of theoretical plates is optimized when $p = p_0$.

By rearranging eq 24 we can obtain

$$N = \frac{\pi^2 \ln 2}{2}\left(\frac{L}{p}\right)^2 / \left\{\eta\left(\frac{\pi^2 DL}{Vp^2}\right)\right\}^2 \tag{26}$$

Based on eq 26, Figure 2 shows normalized N for a fixed p as a function of the V/D value normalized by $\pi^2 L/p^2$. The normalized value of V/D becomes unity when the fixed value of p agrees with values of the characteristic pitch. The value of N is normalized to be unity when normalized V/D is unity. The results suggest guidelines for multicomponent analysis. In the case of multicomponent systems, the perfect optimization of p for all components is impossible because the characteristic pitch is different for each component. As shown in Figure 2, employing the pitch optimized for the smallest value of V/D, we can obtain larger values of N for all components than the value for the component, for which the pitch is optimized.

Error in Power Spectrum Estimation. The power spectrum is defined using infinite time, whereas actual measurements must be completed within finite time. The power spectrum estimated from finite-length data includes unavoidable random errors (noise). If the magnitude of this noise is evaluated by the coefficient of variation (CV), which is defined as the standard deviation normalized by the power spectrum, then

$$\mathrm{CV} = 1/\sqrt{T\Delta f} \tag{27}$$

where T is the data length and Δf is the resolving frequency in the power spectrum estimation.[36]

Aside from random errors, the actual power spectrum of photocurrent fluctuations includes systematic errors (background) arising from shot noise and thermal noise associated with the feedback resistance of the amplifier that follows the detector. This background is a white spectrum given by[39]

$$B(f) = B \equiv 2ge(\langle i \rangle + i_B) + 4k_B T_e/R \tag{28}$$

where g is the gain of the detector, e is the elementally charge, i_B is the average background current (the sum of the dark current of the detector and the photocurrent induced by the background light), k_B is a Boltzmann constant, T_e is the noise equivalent temperature of the amplifier, and R is the feedback resistance. Here we define the signal-to-background ratio, S/B, by $S(f_0)/B$.

(37) Belafhal, A. *Opt. Commun.* **2000**, *177*, 111−118.
(38) Karger, B. L.; Snyder, L. R.; Horvath, C. *An Introduction to Separation Science*; J. Wiley and Sons: New York, 1973; pp 136−137.
(39) Yariv, A. *Optical Electronics*, 4th ed.; Saunders College Publ.: Philadelphia, PA, 1991; Chapter 10.

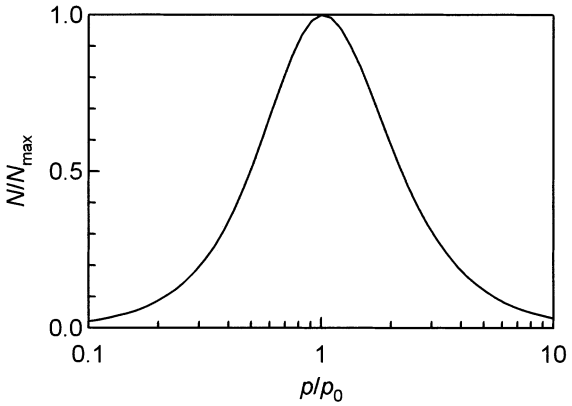

Figure 1. Relation between the normalized number of theoretical plates (N) and the normalized pitch of the excitation pattern (p) in CE/patterned FCS. The normalization factor for N and p are $N_{max} \equiv VL/6.38D$ and $p_0 \equiv \pi(LD/V)^{1/2}$, respectively. Here L is the length of the detection volume along the analyte flow, and V and D are the electrophoretic velocity and the diffusion coefficient of the analytes, respectively.

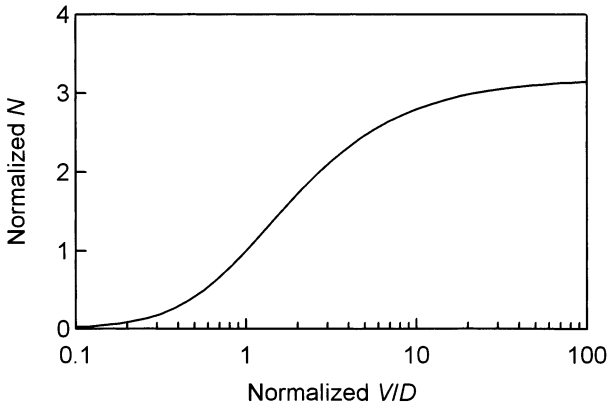

Figure 2. Normalized N for a fixed p as a function of VlD normalized by π^2L/p^2. The value of N is normalized to be unity when normalized VlD is unity.

Since the CV described above is the coefficient not of $S(f)$ but of $S(f) + B$, the noise amplitude is commensurate with $S(f) + B$. To keep the peak of $S(f)$ unaffected by the background noise, $S/B \gg 1$ is required. This condition is particularly important with multicomponent systems, where the background is the sum of those arising from each component. Note that even if $S/B \gg 1$ is satisfied, the noise term commensurate with $S(f)$ remains. However, because this noise vanishes except in the vicinity of f_0, if $S/B \gg 1$, even if CV $\ll 1$ is not satisfied, peak detection is possible.

To obtain a simple and convenient expression for S/B, we approximate the peak profile of $S(f)$ by using a Lorentzian whose area and fwhm are identical to those of the real profile. Because the peak area equals $\langle \delta i^2 \rangle / 3$, we obtain

$$S(f_0) = 2\langle \delta i^2 \rangle / 3\pi w_{1/2} \tag{29}$$

This approximation gives rather smaller values than an exact calculation gives. The relative error is less than 1/3, and it is sufficiently small to estimate the order of S/B. By using eqs 4, 28, and 29, we can write

$$S/B \equiv \frac{S(f_0)}{B(f_0)} = \frac{n_e}{3\pi w_{1/2}} \frac{1}{1 + \dfrac{i_B + 2k_B T_e / geR}{gen_e \bar{C} v}} \tag{30}$$

where

$$n_e \equiv \frac{\langle i \rangle}{eg\langle n \rangle} = \frac{Q\Phi\sigma\phi_0}{2\sqrt{2}} \tag{31}$$

As seen from this definition, n_e is the average number of photoelectrons in the detector per unit of time before the multiplication induced by fluorescence emitted from an analyte molecule. If $\bar{C}$ is so large that

$$i_B \ll gen_e \bar{C} v = \langle i \rangle \tag{32}$$

$$2k_B T/(ge)^2 R \ll n_e \bar{C} v \tag{33}$$

then eq 30 results

$$S/B = n_e / 3\pi w_{1/2} \cong 0.11(n_e / w_{1/2}) \tag{34}$$

Thus, S/B increases with increasing analyte concentration but converges to a constant value commensurate with n_e. To make n_e greater, a high-quantum-efficiency detector must be used as well as robust and bright fluorophores, high excitation power, and bright optical systems for fluorescence collection. Cyanine and rhodamine dyes, major classes of robust and bright fluorophores, emit light whose wavelength is longer than 500 nm. In such a wavelength region, the quantum efficiency of a Si PD is greater than 80%, whereas that of a PMT is less than 20%. Therefore, in theory, a Si PD is better than a PMT as a detector in CE/patterned FCS. However, it should be noted that a very large value of R may be required for a PD to satisfy eq 33 because $g = 1$.

NUMERICAL SIMULATIONS

Number of Theoretical Plates. To compare CE/patterned FCS with conventional CE, we characterize the $1/e^2$ width of the detection volume along the capillary (L) as the effective length in this new technique. If we neglect the detection length, the wall interaction, and the Joule heating effect, the number of theoretical plates obtained by conventional CE using effective length L can be written by[9]

$$N_0 = \frac{VL}{2D} \frac{1}{1 + Vl^2/24DL} \tag{35}$$

where l is the injection length. Figure 3 shows N_{max}, N_0, and p_0 as functions of L, which were numerically computed based on eqs 17, 25, and 35. The assumed parameters are $D = 4 \times 10^{-8}$ cm^2/s, $V = 400$ μm/s, and $l = 100$ μm, typical values for capillary gel electrophoresis of DNA using microfabricated devices.[9] The number of theoretical plates obtained by optimized CE/patterned FCS is superior to that obtained by conventional CE when the effective length is shorter than 1 cm. In this case, the values of the characteristic pitch that optimize CE/patterned FCS range

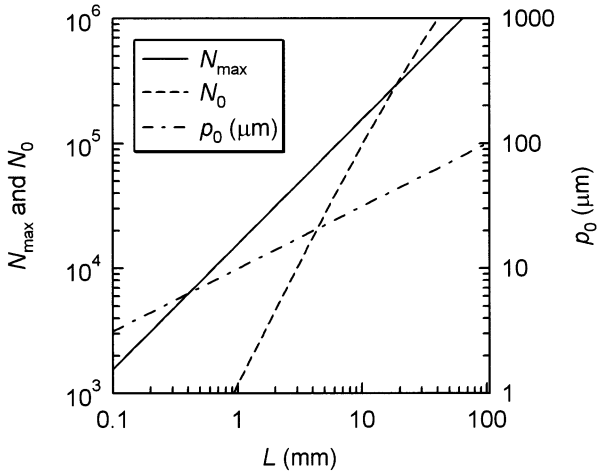

Figure 3. Computed values of the number of theoretical plates in optimized CE/patterned FCS, that in conventional CE, and the characteristic pitch optimizing CE/patterned FCS as functions of effective length L. Assumed parameters are $D = 4 \times 10^{-8}$ cm^2/s, $V = 400$ μm/s, and injection length $l = 100$ μm.

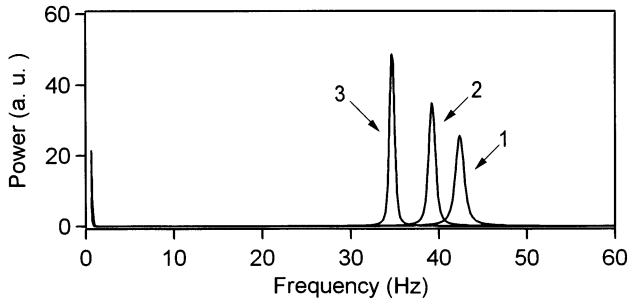

Figure 4. Computed power spectra of fluctuations in the fluorescence intensity from three different analytes migrating under identical conditions. Assumed parameters common for all analytes are $L = 700$ μm, $p = 10.2$ μm, and $E = 200$ V/cm. Other parameters are shown in Table 1.

Table 1. Assumed Parameters for Computing the Spectra Shown in Figure 4 and Computed Values of the Number of Theoretical Plates for Each Peak

	no. of analytes		
	1	2	3
mobility μ (10^{-4} cm^2 V^{-1} s^{-1})	2.16	2.00	1.79
diffusion coefficient D (10^{-8} cm^2 s^{-1})	6.48	4.00	2.12
no. of theoretical plates N	7300	10400	14200

from several micrometers to several tens of micrometers, adequate values that are obtained with the interference of visible light.

Figure 4 shows the computed spectra of fluctuations in the fluorescence intensity from three different analytes migrating under identical conditions. The common parameters for all analytes are $L = 700$ μm, $p = 10.2$ μm, and $E = 200$ V/cm. Other parameters are shown in Table 1. Table 1 also shows computed values of the number of theoretical plates obtained for each analyte. These analytes simulate double-stranded DNAs of 200, 300, and 500 base pairs based on ref 9. While the value of p is optimized for the first analyte, excellent discrimination can be seen in Figure 4. If the sample is a mixture of these analytes, we would obtain a superposed spectrum with essentially perfect separation between all the peaks.

Table 2. Numerically Simulated Values of S/B and n_e and Assumed Parameters

	case number		
	1	2	3
excitation			
wavelength (nm)	488	488	633
total power (mW)	1	1	5
detector			
type	PMT	PMT	Si PD
quantum efficiency Q	0.1	0.1	0.8
gain g	5×10^5	5×10^5	1
feedback resistance (Ω)	10^6	10^6	10^{10}
fluorophore			
name	TOTO-1	fluorocein	Cy5
extinction coefficient ϵ ($cm^{-1}M^{-1}$)	69 000	70 000	175 000
quantum yield Φ	0.34	0.92	0.28
no. of photoelectron per molecule per s n_e (s^{-1})	2.8	7.8	310
signal-to-background ratio S/B	0.34	0.92	36

Here we point out that the advantages of CE/patterned FCS are not only in the abbreviation of separation columns. Another important feature of this technique is its applicability to continuously flowing analytes, which allows the use of a simple sequence in using electric fields and channel structures without special injectors. As seen from eqs 25 and 35, N_{max} is about 1/3 of N_0 when l is sufficiently small. Even in such a case, the advantages of CE/patterned FCS are not necessarily lost, for the reasons explained above.

Signal-to-Background Ratio. The signal-to-background ratio of a photocurrent spectrum is estimated using numerical examples. We can express σ and ϕ_0 as

$$\sigma = \epsilon \ln 10 / N_A \tag{36}$$

$$\phi_0 = \frac{8P_0}{\pi LH(hc/\lambda)} \frac{1 - \sqrt{1 - (NA/n_o)^2}}{2} \bar{T} \tag{37}$$

where ϵ is the molar extinction coefficient of the analyte, N_A is Avogadro's number, h is a Plank constant, c is the velocity of light, P_0 is the total power of the excitation beam, NA is the numerical aperture of the fluorescence collection lens, n_o is the refractive index of the migration matrix in the capillary, and $\bar{T}$ is the mean transmittance of the detection optics for fluorescence. We assumed isotropic fluorescence emission and the use of a dry objective as the collection lens. Substituting eqs 36 and 37 into eq 31 gives

$$n_e = \frac{2\sqrt{2} \ln 10}{\pi} \frac{Q\Phi P_0 \epsilon}{LHN_A hc/\lambda} \frac{1 - \sqrt{1 - (NA/n_o)^2}}{2} \bar{T} \tag{38}$$

Table 2 shows numerically simulated values of n_e and S/B based on eqs 34 and 38 and assumed parameters for the simulation. We assumed that eq 32 is satisfied. The values of ϵ and Φ are nominal values provided by reagent makers.[40,41] The

(40) http://www.probes.com/handbook/.
(41) http://www.amershambiosciences.com/.

common parameters for all cases are $L = 700\ \mu$m, $H = 30\ \mu$m, NA = 0.75, $n_o = 1.33$, $\bar{T} = 35\%$, $T_e = 350$ K, $\bar{C}/N_A = 10$ nM, and $w_{1/2} = 0.9$ Hz. The value of $w_{1/2}$ is identical to that obtained for analyte 2 in the preceding chapter. Equation 33 is well satisfied for all the cases. Cases 1 and 2 simulate the experimental setup described below. The S/B value is less than 1 in both the cases. Thus, peak detection in the photocurrent fluctuation spectrum is difficult in the case of a single chromophoric analyte. However, in the case of intercalators such as TOTO-1, a number of dye molecules can combine with an analyte molecule. Comparing a TOTO-1-stained DNA solution and a fluoroscein solution using a fluorophotometer, we found that TOTO-1 complexes with DNA at a ratio of 1 TOTO-1/13 bp. Therefore, a sufficiently large S/B can be obtained for kilobase-pair DNA. In case 3, an S/B value of 36, which is 106 times greater than that for TOTO-1 in case 1, is obtained for a single Cy5 dye without assuming unrealistic parameters (the R value of $10^{10}\Omega$ is very large but not unrealistic). This result suggests that a single chromophoric analyte can be detected by CE/patterned FCS. If $S/B \sim 36$ for one-component systems of analytes labeled with a single Cy5, the simultaneous detection of such analytes in several-component systems would be possible.

EXPERIMENTAL SECTION

Reagents. A 1× TBE (89 mM Tris, 89 mM boric acid, and 1 mM EDTA) buffer containing no polymers and a 0.5× TBE buffer containing 0.3 wt % hydroxyethylcellulose (HEC, MW = 250 000) buffer were used as the electrophoresis buffer. pUC18 DNA (2686 bp) and λ DNA (48 502 bp) were purchased from Takara. The pUC18 DNA was digested by *Eco*RI so that it became linear double-stranded DNA. TOTO-1 was purchased from Molecular Probes. We prepared 1.25 μg/mL DNA solutions and a 0.1 μM TOTO-1 solution by dilution in the 1× TBE buffer. Solutions of TOTO-1-stained DNA were prepared by 30-min incubation after mixing 10 μL of each DNA solution and 150 μL of the TOTO-1 solution. As a result of intercalation of the TOTO-1 into the double-stranded DNA, stable fluorescent complexes were formed. A solution of TOTO-1-stained pUC18 DNA, a solution of TOTO-1-stained λ DNA, and a mixture of the two former solutions were prepared. The λ DNA-to-pUC18 DNA ratio in the mixture was 1/18. The total DNA concentration in each solution was adjusted to 39 ng/mL by dilution in the 1× TBE buffer or distilled water prior to electrophoresis. In each electrophoresis experiment, the TBE concentration in the DNA solution was equalized with that of the electrophoresis buffer.

Instrumentation. A schematic diagram of the CE/patterned FCS experimental setup is shown in Figure 5. A continuous-wave Ar ion laser (model 2011 20SL, Uniphase) operating at 488 nm was used for fluorescence excitation. The output Gaussian beam of the laser was passed through an optical band-pass filter, BPF1 (FITCA-40, Schott), to enhance its spectral purity and was divided 50/50 on a horizontal plane using a beam splitter into two beams, designated as B_1 and B_2 in Figure 5. Transmitted beam B_2 was reflected from a mirror, and it intersected with reflected beam B_1 at an angle of 2.64° to create an interference pattern. A 22-cm-long, 50 × 50-μm^2 inner cross-section capillary (WWP050300, Polymicro) was placed horizontally in such a way that it met at a

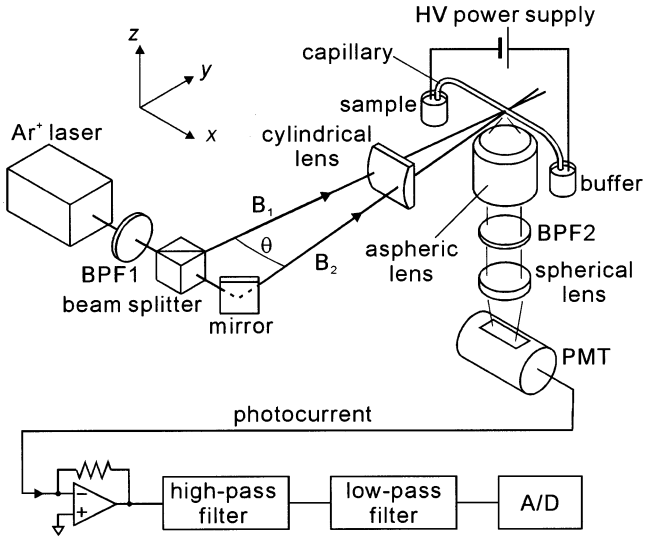

Figure 5. Schematic diagram of the CE/patterned FCS experimental setup. BPF, HV, PMT, and A/D stand for band-pass filter, high voltage, photomultiplier tube, and analog−digital conversion card, respectively.

right angle with the bisection of the angle made by B_1 and B_2 at the intersection point of the two beams. To obtain high excitation efficiency, the beams incident on the capillary were vertically focused into a $1/e^2$ diameter of ~30 μm using a cylindrical lens (f = 30 mm). The horizontal $1/e^2$ diameter and the total power of the incident beams were 740 μm and 1 mW, respectively. The polyimide coating of the capillary in the vicinity of the incident point was removed by burnout to create a 10-mm-wide window. In the geometry described above, the interference pattern pitch, p, in the detection volume is given independently of the refractive index of the capillary wall and the inner medium by using aerial values of the laser wavelength and the intersecting angle as λ and θ in the right-hand side of eq 8. Thus, p was calculated to be 10.6 μm.

The fluorescence emission from the detection volume in the capillary was collected orthogonally to the horizontal plane and collimated using an aspheric lens (01LAG111, Melles Griot, f = 12 mm). The collimated fluorescence was passed through an optical band-pass filter, BPF2 (FITCE-45, Schott), and was weakly focused onto the cathode of the PMT (H5784-01, Hamamatsu) using a spherical lens (f = 30 mm). Since the detection system had no slit, the capillary itself played the role of a 50-μm-wide slit.

Adopting a coordinate system where the x-axis is the capillary axis around the detection volume and the y-axis is the bisection of the incident beams, we can express the MDE profile by the right-hand side of eq 9, where $L = 740\ \mu$m, $p = 10.6\ \mu$m, $H = 30\ \mu$m, and $W = 50\ \mu$m.

The capillary and the buffer reservoir were filled with the buffer, and the sample reservoir was filled with TOTO-1-stained DNA solutions. The inlet and the outlet of the capillary were immersed into the sample reservoir and the buffer reservoir, respectively. Electric fields of 50−200 V/cm were applied between the reservoirs using a high-voltage power supply (model HCZE-30PN0.25-LDS, Matsusada) capable of supplying 0−30 kV. The electrokinetically injected DNA from the sample reservoir migrated through the capillary in the directions of the buffer

reservoir. The fluorescence emission from the DNA arriving at the detection volume was monitored by the PMT.

The photocurrent of the PMT was converted into a voltage using a PMT-adapted transimpedance amplifier with a gain of 1 MΩ. The output signal of the amplifier was passed through a high-pass filter (model 3611, NF) and a low-pass filter (RT-8FLA1, NF) and was acquired at the 250-Hz sampling rate and 16-bit resolution on a personal computer through an analog−digital conversion card (AT-MIO-16X, National Instruments) with a program written in LabVIEW 4.1 (National Instruments). The output signal of the amplifier before it was input into the high-pass filter was always monitored using an oscilloscope. The gain of the high-pass filter was within ±0.5 dB over 0.2 Hz and that of the low-pass filter was within ±0.5 dB from dc to 96 Hz and less than −80 dB over 150 Hz. Therefore, our signal conditioning system could perform spectral analysis with an accuracy of ±0.7 dB from 0.2 to 96 Hz without alias.

Procedures. All experiments were carried out at room temperature. We started the electrokinetic injection of DNA at 200 V/cm. Within a few minutes, the arrival of the TOTO-1-stained DNA in the detection volume raised the output signal of the amplifier. After the rise abated, the output signal of the low-pass filter was acquired at several values of the electric field. The power spectrum of the photocurrent fluctuations was estimated by using an average of 10 periodograms. Each periodogram was calculated from a fast Fourier transform of 1024-point data acquired during 4.1 s. Further, the averaged periodograms were smoothed with IGOR 3.14 (WaveMetrics), using a 1-pass polynomial algorithm. As a result, the data length used to estimate the spectrum and the resolving frequency in the estimation were 41 s and 0.49 Hz, respectively.

RESULTS AND DISCUSSION

Figure 6 shows the power spectra of fluctuations in the fluorescence intensity from the TOTO-1-stained pUC18 DNA electrophoretically migrating in the 1× TBE buffer containing no polymers at electric fields of 50, 100, 150, and 200 V/cm. The peak frequency f_0 increased linearly with the electric field E. This result is consistent with ref 42, where the mobility of DNA does not depend on E. The mobility was calculated to be 3.5×10^{-4} $cm^2\ V^{-1}\ s^{-1}$ by using the value of p (10.6 μm) and linear regression between E and f_0 based on eq 22. This mobility value is also reasonable.

We assume that the fwhm w_{total} of the peak in the observed spectrum is given by

$$w_{total}^2 = w_{1/2}^2 + \Delta f^2 \qquad (39)$$

where $w_{1/2}$ is the real fwhm of the photocurrent fluctuation spectrum, which is theoretically predicted by eq 19, and Δf is the resolving frequency in the spectrum estimation, which was 0.49 Hz. Figure 7 shows a plot of plate number N versus electric field E. The open circles and the solid line represent, respectively, the experimentally obtained values and the theoretical values calculated using eq 39 and the experimentally determined mobility.

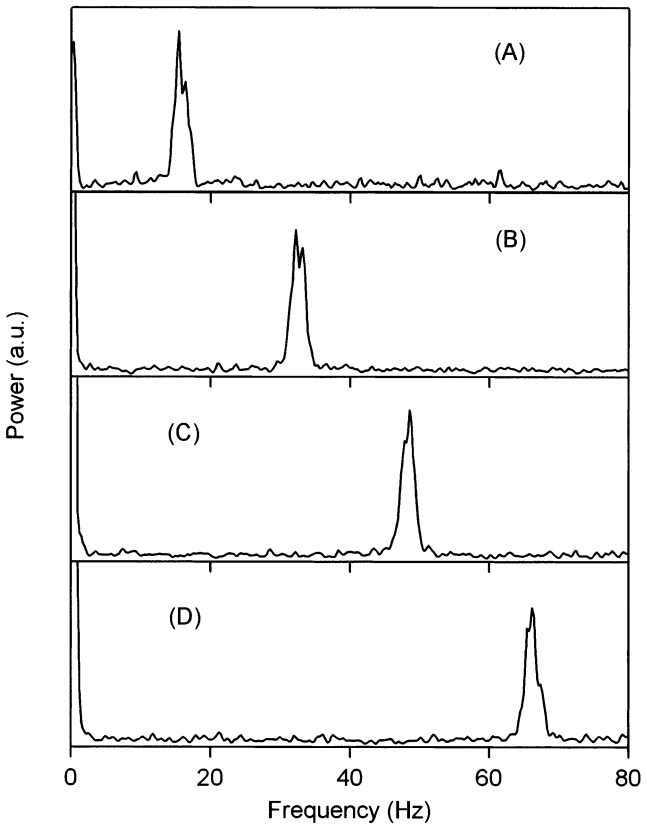

Figure 6. Power spectra of fluctuations in the fluorescence intensity from TOTO-1-stained pUC18 DNA migrating in the 1× TBE buffer containing no polymers at electric fields of 50 (A), 100 (B), 150 (C), and 200 V/cm (D).

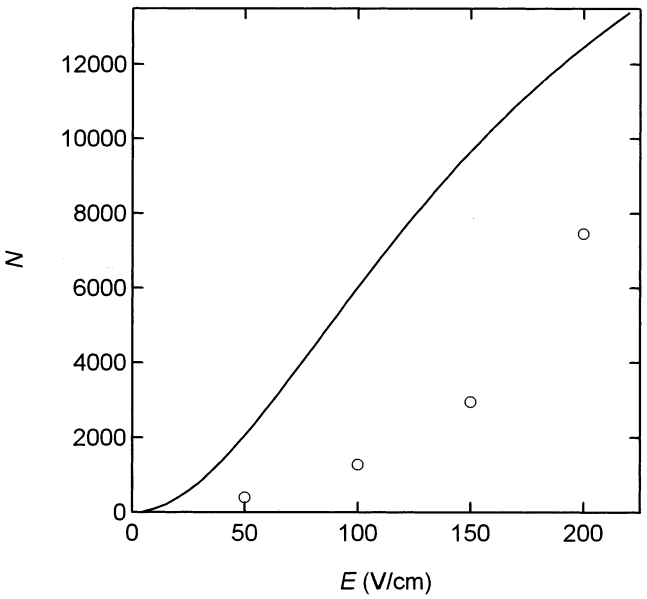

Figure 7. Plate number N of peaks in Figure 6 vs electric field E. The open circles and the solid line respectively represent the experimentally obtained values and the theoretical values calculated by using eq 24 and the experimentally determined mobility of pUC18 DNA.

According to ref 42, we assumed that $D = 3 \times 10^{-8}$ $cm^2\ s^{-1}$, for which the condition of eq 11 is satisfied. The experimental values are appreciably smaller than the theoretical values. In other words, the experimentally obtained peaks are wider than the theoretically

(42) Nkodo, A. E.; Garnier, J. M.; Tinland, B.; Ren, H.; Desruisseaux, C.; McCormick, L. C.; Drouin, G.; Slater, G. W. *Electrophoresis* **2001**, *22*, 2424−2432.

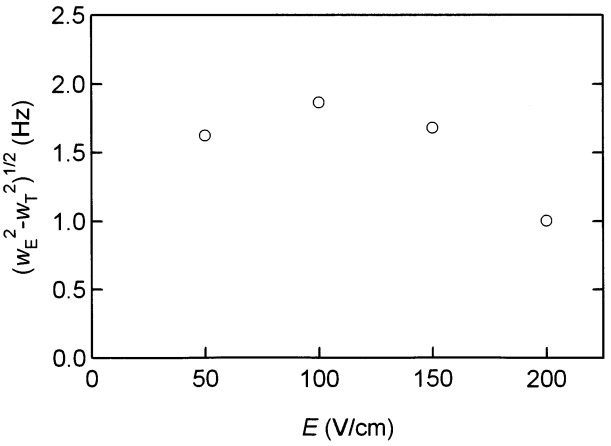

Figure 8. Excessive peak broadening, $(w_E^2 - w_T^2)^{1/2}$, vs electric field E. Here w_E and w_T are the experimental value and the theoretical value of fwhm, respectively.

predicted ones. Here we define the excessive peak broadening by $(w_E^2 - w_T^2)^{1/2}$, where w_E and w_T are the experimental value and the theoretical value of fwhm, respectively. Figure 8 shows a plots of $(w_E^2 - w_T^2)^{1/2}$ versus E. If this broadening originated in the mobility shift caused by the temperature drift during the data acquisition, it should be proportional to the electric field. However, it is actually not so. At present, we cannot fully explain the origin of the peak broadening. One possible explanation lies in excitation pattern fluctuations caused by vibrations of the optical system. Since the system is composed of a two-beam interferometer, its vibration easily yields excitation pattern fluctuations, which would modulate the fluorescence correlation and broaden the peaks in the power spectrum.

As described above, the theoretical limit has not been achieved. Nevertheless, 7400 theoretical plates were obtained at 200 V/cm, using an effective length of 740 μm. This value corresponds to a plate height (L/N) of 0.1 μm. Such high efficiency is epochal in submillimeter effective length CE.

Despite the broadening of the peaks, their area does not change because it corresponds to the total power of the modulated component of the photocurrent. Therefore, eq 34 would work if $w_{1/2}$ is replaced with experimentally measured fwhm as long as the shape of the peaks does not significantly deviate from Lorentzian. On this basis, we estimate the S/B in the case of Figure 6D as an example. Assuming 200 TOTO-1 molecules complex with a pUC18 DNA molucule, S/B is calculated to be 34 from n_e in Table 2 and the measured fwhm (1.8 Hz) by using eq 34. The actual value of S/B in Figure 6D is 20, the order of which agrees with the calculated value.

Figure 9 shows the power spectra of fluctuations in the fluorescence intensity from the TOTO-1-stained DNA electrophoretically migrating in the 0.5× TBE buffer containing 0.3% HEC at an electric field of 200 V/cm. The samples from which DNA was injected are the solution of pUC18 DNA (A), the solution of λ DNA (B), and the mixture (C). In Figure 9C, two peaks corresponding to two analytes were clearly separated, though the resolution is not perfect. The number of plates of peaks in Figure 9 is not as high as in Figure 6D, but it exceeds 1000, which cannot be readily obtained in conventional CE using the submillimeter effective length. To discuss the resolution in Figure 9C quantitatively, pUC18 DNA and λ DNA are defined as the first and second

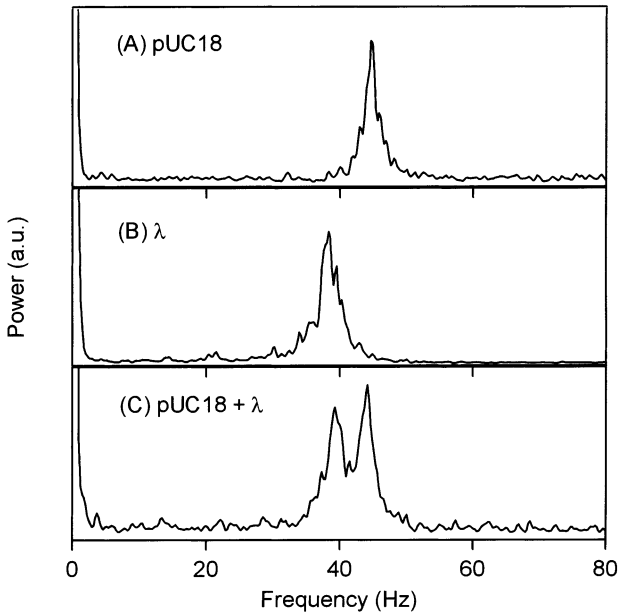

Figure 9. Power spectra of fluctuations in fluorescence intensity from the TOTO-1-stained DNA electrophoretically migrating in the 0.5× TBE buffer containing 0.3% HEC at an electric field of 200 V/cm. The samples from which DNA was injected are the solution of λ DNA (A), the solution of pUC18 DNA (B), and the mixture (C).

components in the mixture solution, respectively, and the fwhm and center frequency of the peak for the ith component are denoted as w_i and f_i, respectively. Then, the resolution, R_S, can be defined by

$$R_S \equiv \sqrt{2 \ln 2}\,\frac{f_1 - f_2}{w_1 + w_2} \tag{40}$$

In Figure 9C, we obtain $R_S = 1.0$.

The diffusion coefficients of pUC18 DNA and λ DNA in TBE buffer containing 0.3% HEC are possibly smaller than that of pUC18 DNA in TBE buffer containing no polymers. On this assumption, the peaks in Figure 9 are considerably wider than theoretically predicted ones, as is the case in Figure 6. Furthermore, the peaks in Figure 9 trail wider skirts than the peaks in Figure 6 do, which deteriorates the separation in Figure 9C. We consider the mobility dispersion of TOTO-1-stained DNA in HEC solutions[43] to be the origin of these skirts.

Here we discuss the relative peak intensity in Figure 9C. For the ith component, $S(f_0)$, B, n_e, and $\bar{C}$ are denoted as S_i, B_i, n_i, and C_i, respectively. Since eqs 32 and 33 were satisfied, $S_i/B_i \propto n_i/w_i$ and $B_i \propto C_i$ are derived from eq 34 and eqs 13 and 28, respectively. As a result, we obtain $S_2w_2/S_1w_1 = n_2C_2/n_1C_1$. In the present case, n_2/n_1 equals the ratio of the baselengths of the components, which is $48502/2686 = 18$. On the other hand, we set $C_2/C_1 = 1/18$. Therefore, we can predict that $S_2w_2 = S_1w_1$. This prediction is supported by the result in Figure 9C.

So far, our experimental demonstration has been limited to the case of comparatively long double-stranded DNA. Our system,

(43) Zhu, H.; Clark, S. M.; Benson, S. C.; Rye, H. S.; Glazer, A. N.; Mathies, R. A. *Anal. Chem.* **1994**, *66*, 1941−1948.

because of its poor sensitivity, can detect only multichromophoric analyte. However, there is further room for improvement in that the quantum efficiency of the detector and the excitation power are not so high in the current system. As predicted in the section on numerical simulations, single chromophoric analytes can, in fact, be detected by CE/patterned FCS in a realistic condition. In the future, we plan to improve the experimental system so that the conditions of excitation and detection agree with case 3 in Table 2, which would enable analyzing DNA labeled at the 5′-end with Cy5. Because unlike intercalator-stained DNA, end-labeled DNA has almost no mobility dispersion, it is a model analyte. We also intend to completely eliminate vibration of the optical system. This will enable us to test our theory under more ideal conditions.

CONCLUSIONS

A new method for electrophoretic analysis has been developed using a combination of CE and patterned FCS. It was theoretically shown that the power spectrum of photocurrent fluctuations results in a virtual electropherogram. Virtual electropherograms were successfully observed in the fluorometry of TOTO-1-stained pUC18 DNA and λ DNA using an effective length of 740 μm. Remarkably high separation efficiency was obtained in submilimeter effective length CE. Although the results of our experiments do not fully agree with the theoretical predictions, the feasibility of a promising new technique has been demonstrated in principle.

The scope of applications of this new combination is not limited to the mere miniaturization of conventional CE/LIF. The high spacial resolution of this technique would enable measurements of the local velocity in various microfluidic devices. An important possibility is the utilization as a high-sensitivity version of electrophoretic light scattering (ELS). Photocurrent fluctuation spectra in CE/patterned FCS is probably compatible with heterodyne spectra in ELS. CE/patterned FCS may be used to analyze chemically reacting components separately in equilibrium states, as well as ELS.[24] In this direction for use, there are many interesting subjects such as the analysis of protein−protein interaction. We expect that this work is a first step toward a wide variety of applications of this new technique.

ACKNOWLEDGMENT

We thank Prof. Toshio Ando, who sent us his unpublished manuscript. The manuscript was very informative. We thank Dr. Yukiko Hirabayashi for her help in the literature search.

APPENDIX

In this section, we derive eq 12. The following discussion is based on ref 24. The normalized correlation function $G(t)$ can be written by

$$G(t) = \frac{\int |\phi(\mathbf{q})|^2 F(\mathbf{q},t)\ \mathrm{d}\mathbf{q}}{\int |\phi(\mathbf{q})|^2 F(\mathbf{q},0)\ \mathrm{d}\mathbf{q}} \tag{A.1}$$

where $\phi(\mathbf{q})$ is the spatial Fourier transform of $\phi(\mathbf{r})$ and $F(\mathbf{q}, t)$ is the correlation function of the spatial Fourier transform of $\delta C(\mathbf{r}, t)$, which are defined by

$$\phi(\mathbf{q}) \equiv \int \phi(\mathbf{r})\ \exp(j\mathbf{q}\cdot\mathbf{r})\ \mathrm{d}\mathbf{r} \tag{A.2}$$

$$\delta C(\mathbf{q},t) \equiv \int \delta C(\mathbf{r},t)\ \exp(j\mathbf{q}\cdot\mathbf{r})\ \mathrm{d}\mathbf{r} \tag{A.3}$$

$$F(\mathbf{q},t) \equiv \langle \delta C(\mathbf{q},0)\delta C(\mathbf{q},t)\rangle \tag{A.4}$$

To simplify the equations, we introduce

$$k \equiv 2\pi/p, \quad \sigma_x \equiv L/4, \quad \sigma_y \equiv W/4, \quad \sigma_z \equiv H/4, \quad \tau_i \equiv \sigma_i^2/D\ (i = x,y,z) \tag{A.5}$$

Substitution of eq 9 into eq A.2 yields

$$\phi(\mathbf{q}) = \phi_0\phi_x(q_x)\phi_y(q_y)\phi_z(q_z) \tag{A.6}$$

where

$$\phi_x(q_x) \equiv \sqrt{2\pi}\sigma_x\left[\frac{1}{2}\exp\left\{-\frac{\sigma_x^2(q_x-k)^2}{2}\right\} + \frac{1}{2}\exp\left\{-\frac{\sigma_x^2(q_x+k)^2}{2}\right\} + \exp\left(-\frac{\sigma_x^2 q_x}{2}\right)\right] \tag{A.7}$$

$$\phi_i(q_i) \equiv \sqrt{2\pi}\sigma_i\ \exp\left(-\frac{\sigma_i^2 q_i^2}{2}\right)\quad (i = y,z) \tag{A.8}$$

$F(\mathbf{q}, t)$ is given by

$$F(\mathbf{q},t) = F(\mathbf{q},0)F_x(q_x,t)F_y(q_y,t)F_z(q_z,t) \tag{A.9}$$

where

$$F_x(q_x,t) \equiv \exp(jq_xVt - q_x^2Dt), \quad F_i(q_i,t) = \exp(-q_i^2Dt)\quad (i = y,z) \tag{A.10}$$

Because k is less than 4×10^5 cm^{-1} as long as visible light is used for fluorescence excitation, $\phi(\mathbf{q})$ vanishes for $\mathbf{q}$ whose magnitude is greater than 10^6 cm^{-1}. On the other hand, away from critical points or phase transitions, $F(\mathbf{q}, 0)$ should be independent of $\mathbf{q}$, whose magnitude is less than 10^6 cm^{-1}. Therefore, we can write

$$G(t) = G_x(t)G_y(t)G_z(t) \tag{A.11}$$

where

$$G_i(t) \equiv \frac{\int |\phi_i(q_i)|^2 F_i(q_i,t)\ \mathrm{d}q_i}{\int |\phi_i(q_i)|^2 F_i(q_i,0)\ \mathrm{d}q_i}\ (i = x,y,z) \tag{A.12}$$

Multiplication of both sides of eq A.7 by themselves results in

$$|\phi_x(q_x)|^2 = 2\pi\sigma_x^2\left[\frac{\exp\{-\sigma_x^2(q_x-k)^2\}}{4} + \frac{\exp\{-\sigma_x^2(q_x+k)^2\}}{4} + \exp(-\sigma_x^2 q_x^2) + \frac{\exp(-\sigma_x^2k^2-\sigma_x^2q_x^2)}{2} + \exp\left\{-\sigma_x^2\left(q_x-\frac{k}{2}\right)^2 - \frac{\sigma_x^2k^2}{4}\right\} + \exp\left\{-\sigma_x^2\left(q_x+\frac{k}{2}\right)^2 - \frac{\sigma_x^2k^2}{4}\right\}\right] \quad \text{(A.13)}$$

Because eq 10 gives $\sigma_x k \gg 1$, all but the first three terms on the right-hand side of eq A.13 can be neglected. As a result, we can write

$$G_x(t) = \frac{G_1(k,t) + G_1(-k,t) + 4G_1(0,t)}{G_1(k,0) + G_1(-k,0) + 4G_1(0,0)} \quad \text{(A.14)}$$

where

$$G_1(k,t) \equiv \int_{-\infty}^{\infty} F_x(q,t)\exp\{-\sigma_x^2(q-k)^2\}\,dq = \frac{\sqrt{\pi}}{\sigma_x\sqrt{1+\frac{t}{\tau_x}}}\exp\left(\frac{jkVt - k^2Dt - \frac{V^2t^2}{4\sigma_x^2}}{1+\frac{t}{\tau_x}}\right) \quad \text{(A.15)}$$

Exact expressions of $G_y(t)$ and $G_z(t)$ are readily obtained by substituting eqs A.8 and A.10 into eq A.12 as follows:

$$G_i(t) = \left(1+\frac{t}{\tau_i}\right)^{-1/2} \quad (i = y,z) \quad \text{(A.16)}$$

Substituting eqs A.14 and A.16 into eq A.11, we obtain

$$G(t) = \frac{1}{\sqrt{1+\frac{t}{\tau_x}}\sqrt{1+\frac{t}{\tau_y}}\sqrt{1+\frac{t}{\tau_z}}}\left\{\frac{1}{3}\cos\left(\frac{kVt}{1+\frac{t}{\tau_x}}\right)\exp\left(\frac{-k^2Dt - \frac{V^2t^2}{4\sigma_x^2}}{1+\frac{t}{\tau_x}}\right) + \frac{2}{3}\exp\left(\frac{-\frac{V^2t^2}{4\sigma_x^2}}{1+\frac{t}{\tau_x}}\right)\right\} \quad \text{(A.17)}$$

Equation 11 equals to $\sigma_x/V \ll \tau_i$ $(i = x, y, z)$, which simplifies eq A.17 to eq 12.

Received for review February 27, 2002. Accepted July 20, 2002.

AC0201326